# Charge carrier scattering and ultrafast Auger dynamics in two-dimensional superatomic semiconductors

Cite as: Appl. Phys. Lett. **116**, 201109 (2020); https://doi.org/10.1063/5.0001839 Submitted: 20 January 2020 . Accepted: 08 May 2020 . Published Online: 21 May 2020

Heejae Kim , Kihong Lee , Avalon H. Dismukes , Bonnie Choi, Xavier Roy , Xiaoyang Zhu , and Mischa Bonn







## ARTICLES YOU MAY BE INTERESTED IN

Strong polaronic effect in a superatomic two-dimensional semiconductor
The Journal of Chemical Physics 152, 171101 (2020); https://doi.org/10.1063/5.0006455

Controlling the dopant profile for SRH suppression at low current densities in  $\lambda \approx$  1330 nm GalnAsP light-emitting diodes

Applied Physics Letters 116, 203503 (2020); https://doi.org/10.1063/5.0002058

Study of vertical hole transport in InAs/InAsSb type-II superlattices by steady-state and time-resolved photoluminescence spectroscopy

Applied Physics Letters 116, 201108 (2020); https://doi.org/10.1063/1.5144888

Lock-in Amplifiers up to 600 MHz







## Charge carrier scattering and ultrafast Auger dynamics in two-dimensional superatomic semiconductors

Cite as: Appl. Phys. Lett. **116**, 201109 (2020); doi: 10.1063/5.0001839 Submitted: 20 January 2020 · Accepted: 8 May 2020 · Published Online: 21 May 2020







Heejae Kim,<sup>1,a)</sup> (i) Kihong Lee,<sup>2</sup> (i) Avalon H. Dismukes,<sup>2</sup> (i) Bonnie Choi,<sup>2</sup> Xavier Roy,<sup>2</sup> (ii) Xiaoyang Zhu,<sup>2</sup> (ii) and Mischa Bonn<sup>1</sup> (ii)

### **AFFILIATIONS**

- <sup>1</sup>Department of Molecular Spectroscopy, Max Planck Institute for Polymer Research, Ackermannweg 10, 55128 Mainz, Germany <sup>2</sup>Department of Chemistry, Columbia University, New York 10027, USA
- <sup>a)</sup>Author to whom correspondence should be addressed: kim@mpip-mainz.mpg.de

### **ABSTRACT**

Superatom solids are promising for optoelectronic applications, owing to their tunable structural and electronic properties; yet, the electronic transport properties of these materials have been largely unexplored. Here, we report the Auger recombination dynamics of free carriers in two representative two-dimensional superatomic semiconductors,  $Re_6Se_8Cl_2$  and  $Mo_6S_3Br_6$ , studied using ultrafast terahertz photoconductivity measurements. The fast Auger recombination dynamics are characterized by a cubic dependence of the Auger rate on carrier density in  $Re_6Se_8Cl_2$  and a quadratic dependence in  $Mo_6S_3Br_6$ . The effective lifetimes of  $Mo_6S_3Br_6$  ( $\sim 0.5$  ps) are over an order of magnitude shorter than those ( $\sim 20$  ps) of  $Re_6Se_8Cl_2$ . These results highlight the variability of the optoelectronic properties of different superatom solids.

Published under license by AIP Publishing. https://doi.org/10.1063/5.0001839

Superatom solids are crystals assembled by molecular clusters as the fundamental building blocks. 1,2 Owing to the possibility to control their chemical compositions, and thereby the geometric and electronic structures, superatom solids have great potential for new materials design. Among such solids are transition metal chalcogenide halides, where the superconductivity in the Chevrel phase<sup>3</sup> and unusual magnetic properties<sup>4</sup> of some compounds have been discovered. The transition metal chalcogenide halides form the cluster structure of  $[M_6L_8]L'_6$ , in which M is a transition metal forming an octahedron  $(M_6)$  and L and L' are halogen- or chalcogenide-ligands bridging the neighboring clusters [Fig. 1(a)]. The characteristic dimensionality of the material depends on the number of bridging ligands between clusters. The isolated  $[M_6L_8]L'_6$  clusters tend to share L' or L site atoms with neighboring clusters, forming one, two, or three-dimensionally extended crystal structures, as the number of ligands per  $M_6$  cluster decreases from the maximum value of 14. For example, Mo<sub>6</sub>S<sub>3</sub>Br<sub>6</sub> and Re<sub>6</sub>Se<sub>8</sub>Cl<sub>2</sub> with 9 and 10 ligands per cluster form 2D layered structures (Fig. 1), respectively. The possibility to tune the cluster compositions and their interactions in superatom solids allows for great variation in properties, such as superconductors (e.g., PbMo<sub>6</sub>S<sub>8</sub> and currentannealed  $Re_6S_8Cl_2$ , 5,6 semiconductors (e.g., Mo<sub>6</sub>S<sub>3</sub>Br<sub>6</sub> Re<sub>6</sub>Se<sub>8</sub>Cl<sub>2</sub>),<sup>7,8</sup> and insulators (e.g., PbMo<sub>6</sub>Cl<sub>14</sub> or Re<sub>6</sub>Se<sub>4</sub>Cl<sub>10</sub>).<sup>5</sup>

Understanding the variety of electronic and magnetic properties derived from the common cluster framework could provide insight into further applications of this type of material. Among attempts to simplify the description of the electronic structure of these various compounds, the so-called three-band model has been proposed from tight-binding band structure calculations. In this simplified picture, the three bands include the filled B1 band, composed almost exclusively of ligand p orbitals (p L), and the energetically higher two bands, of the metal d orbitals (d M) in M<sub>6</sub> clusters: the B2 band made of 12 d M levels and the B3 band of 18 d M levels [Fig. 1(f)]. As the Fermi level lies in the B2 band or between the two metal d bands, the number of electrons in the metallic cluster determines the electronic properties. The gap between the two metal d bands is sensitive to the ligand configuration, consistent with ligand field theory. Still, ultrafast carrier dynamics in many of these materials are largely unexplored.

Here, we study two prototypical 2D superatomic solids: <sup>10</sup> Re<sub>6</sub>Se<sub>8</sub>Cl<sub>2</sub> and Mo<sub>6</sub>S<sub>3</sub>Br<sub>6</sub> single crystals<sup>7,8,11</sup> to investigate the ultrafast charge carrier dynamics using time-resolved optical-pump terahertz (THz)-probe spectroscopy. Re<sub>6</sub>Se<sub>8</sub>Cl<sub>2</sub> is an indirect bandgap semiconductor with a bandgap of 1.49<sup>7</sup> eV and the estimated exciton binding energy of 100 meV. Mo<sub>6</sub>S<sub>3</sub>Br<sub>6</sub>, on the other hand, has a direct bandgap of 1.65 eV, <sup>8</sup> and the exciton binding energy is unknown. Analogous to

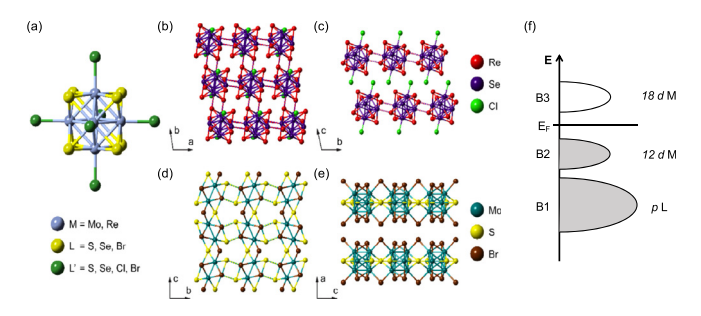


**FIG. 1.** (a) The common structure formula  $[M_6L_8]L_6'$ , where M is a transition metal forming an octahedron and L and L' are halogen- or chalcogenide-ligands bridging with other clusters. (b) and (c) Crystal structure of  $Re_6Se_8Cl_2$ . Top view [(b), ab plane] of a single layer and side view [(c), bc plane]. (d) and (e) Crystal structure of  $Mo_6S_3Br_6$ . Top view [(d), bc plane] of a single layer and side view [(e), ac plane]. (f) The schematic of the simplified three-band model.

the 2D transition metal dichalcogenides, 12-14 these materials have potential applications in light emitters, photodetectors, and solar cells. The electron dynamics and the quantum efficiency of such devices are determined by carrier recombination processes. 15 In particular, for light-emitting diodes (LED) and laser-oriented applications, the devices usually suffer from the reduction in the quantum efficiency at high current densities. 16,17 At high carrier densities, the Auger process is a pronounced carrier recombination mechanism among several non-radiative relaxation processes. In the Auger process, an electron and a hole recombine by transferring the released excess energy to a third carrier, rather than emitting a photon. For improving the device efficiency, it is important to understand and control the Auger recombination process. Thus, we focus on carrier recombination dynamics at high carrier densities above the Mott density of Re<sub>6</sub>Se<sub>8</sub>Cl<sub>2</sub>. For Mo<sub>6</sub>S<sub>3</sub>Br<sub>6</sub>, the free charge carriers are unambiguously observed to be main photoproducts at the same excitation densities.

In order to investigate the recombination processes, we photoin-ject charge carriers with femtosecond pulses with photon energies close to (1.55 eV) and above (3.10 eV) the bandgap of the material and monitor the subsequent charge carrier dynamics by ultrafast THz spectroscopy. The differential transmittance of THz pulses before and after photoexcitation directly reflects the photoconductivity of the sample. Moreover, by scanning the time delay of THz pulses relative to the excitation pulses, the time evolution of the photoconductivity is recorded. The experimental data analyzed based on a rate equation of the carrier density relaxation reveal a dominant third-order process in  $\rm Re_6Se_8Cl_2$  and a limiting second-order Auger process in  $\rm Mo_6S_3Br_6$  with several orders of magnitude shorter effective lifetime.

The transport properties of these photoinjected charge carriers are observed from the photoinduced change in THz transmittance at a specific pump time delay. The transient frequency-dependent complex photoconductivity  $(\tilde{\sigma}(\omega))$  is extracted from the Fourier transforms of the differential THz waveform  $(\Delta \tilde{E}(\omega))$  and the transmitted waveform through the unexcited sample  $(\tilde{E}(\omega))$ . Since the initial distribution of the photoproducts is constrained by the optical penetration depths ( $\sim$ 140 and  $\sim$ 50 nm for 800 and 400 nm excitations in Re<sub>6</sub>Se<sub>8</sub>Cl<sub>2</sub>, respectively<sup>7</sup>), we use an analytical thin-film approximation as follows: <sup>18,19</sup>

$$\frac{\tilde{E}(\omega) + \Delta \tilde{E}(\omega)}{\tilde{E}(\omega)} = \frac{n+1}{n+1 + Z_0 \tilde{\sigma}(\omega) d},$$

where n is the index of refraction of the substrate at THz frequency,  $Z_0$  is the impedance of free space (377  $\Omega$ ), and d is the thickness of the conductive layer. The sample consists of single crystals with lateral dimensions of a few hundreds  $\mu$ m and thicknesses of 20–100  $\mu$ m, deposited on a polymer substrate. In processing the data, we assume that each sample is a thin slab of excited material in a homogeneous dielectric medium with semi-infinite transverse dimensions <sup>18,19</sup> and ignore the surface roughness. We note that due to the carrier diffusion, the thickness of the conductive layer d is a parameter that depends on time after excitation, as will be discussed further below.

At all studied fluence, the photogenerated carrier densities are  $2\times 10^{18}\sim 4\times 10^{19} cm^{-3}$ , which exceed the estimated Mott density of  $Re_6Se_8Cl_2$  (2  $\times 10^{18} cm^{-3}$ ). Although the layered semiconductors, such as  $Re_6Se_8Cl_2$  and  $Mo_6S_3Br_6$ , tend to have non-negligible exciton binding energies at room temperature, beyond a critical density, the bound electron–hole pairs undergo ionization: the Mott transition.  $^{20}$  The Mott density of  $Re_6Se_8Cl_2$  is inferred from the screening length in the classical limit,  $^{21}$  with the reported dielectric constant (at 1.5 eV) and the exciton binding energy of  $\sim\!100\,\text{meV}^7$ . As evident in Fig. 2, the photoconductivity reflects that free charge carriers are the major photoproducts.

Figure 2 shows the extracted real and imaginary parts of the complex conductivity,  $\text{Re}[\tilde{\sigma}]$  and  $\text{Im}[\tilde{\sigma}]$ , in the 0.4–1.6 THz region, at t=10 ps (in  $\text{Re}_6\text{Se}_8\text{Cl}_2$ ) and 1.5 ps (in  $\text{Mo}_6\text{S}_3\text{Br}_6$ ) after the excitation pulse at 84 K. Both spectra display a substantial  $\text{Re}[\tilde{\sigma}]$ , showing significant contribution from free carriers—for excitons, only an imaginary response would be expected at these low frequencies. The negative sign of the imaginary components is typical for charge mobility under confinement, which can be well described by the Drude–Smith (DS) model (Fig. 2). In this generalized form of the Drude model, suppression of the conductivity by preferential backward scattering of electrons (as a result of reflecting from grain boundaries/defects or Coulombic force) is taken into account and imaginary parts of the complex components.

$$\tilde{\sigma}(\omega) = \frac{Ne^2 \tau}{m^* (1 - i\tau\omega)} \left( 1 + \sum_{n=1}^{\infty} \frac{c_n}{(1 - i\tau\omega)^n} \right), \tag{1}$$

where N is the carrier density,  $\tau$  is the scattering time,  $m^*$  is the effective mass, and  $c_n$   $(-1 < c_n < 0)$  is the persistence or memory of the

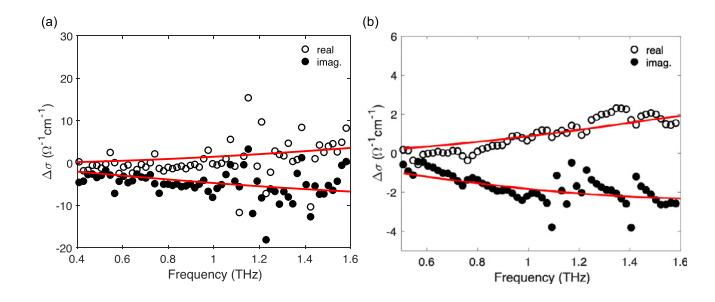


**FIG. 2.** Complex photoconductivity spectra of Re<sub>2</sub>Se<sub>8</sub>Cl<sub>2</sub> (a) and Mo<sub>6</sub>S<sub>3</sub>Br<sub>6</sub> (b) obtained at the time delay of t = 10 and 1.5 ps, respectively, after 800 nm excitation at 84 K. Red lines show the results of the Drude–Smith model, with charge carrier scattering times of  $\sim\!25$  fs and  $\sim\!36$  fs, respectively (see the main text for details).

carrier velocity, i.e., the fraction of the electron's original velocity that is retained after the nth collision. For  $c_n = 0$ , the velocity is completely randomized at each scattering event, while for  $c_n = -1$ , scattering preferentially occurs in the back-direction.

The solid red lines in Fig. 2 are the result of applying this DS model with the carrier effective mass,  $1/m^* = 1/m_e^* + 1/m_h^*$ , in which the effective electron and hole masses are  $m_e^* = 1.15 m_e$  and  $m_h^* = 0.66 m_e$ . We assume unity photon-to-free-charge conversion efficiency. The scattering times of Re<sub>6</sub>Se<sub>8</sub>Cl<sub>2</sub> and Mo<sub>6</sub>S<sub>3</sub>Br<sub>6</sub> obtained using the DS model are  $\sim$ 25 fs with c = -1 and  $\sim$ 36 fs with c = -1, respectively. The corresponding averaged infrared mobilities are  $\sim$ 105 cm<sup>2</sup>/V·s and  $\sim$ 150 cm<sup>2</sup>/V·s, respectively. We note that since the effective mass is only available for Re<sub>6</sub>Se<sub>8</sub>Cl<sub>2</sub><sup>7</sup> and the fit parameter for the scattering time is not sensitive to the effective mass, we use the same value for Mo<sub>6</sub>S<sub>3</sub>Br<sub>6</sub>. In this experimental condition of high photoelectron densities, the mobilities may be affected by charge-charge scattering.<sup>24–26</sup> However, these charge-charge interactions are suppressed in polar semiconductors such as Re<sub>6</sub>Se<sub>8</sub>Cl<sub>2</sub> and Mo<sub>6</sub>S<sub>3</sub>Br<sub>6</sub>. For instance, the scattering rate of TiO2, an example of polar semiconductors, is density-independent up to  $\sim 10^{18} \, \mathrm{cm}^{-3}$ . Thus, we assume that the scattering rate is constant in the entire fluence range.<sup>24</sup>

The relaxation dynamics of the charge carriers appears as the temporal evolution of the differential THz transmittance after the photoexcitation. Figure 3 shows the measured average dynamics,  $\Delta E(\tau,t_{peak})$ , in Re<sub>6</sub>Se<sub>8</sub>Cl<sub>2</sub> as a function of delay time ( $\tau$ ) after the excitation pulse, at the peak of the THz pulse ( $t=t_{peak}$ ). At around 0 <  $\tau$  < 1 ps, we find a pulse-duration-limited rise of the signal, along with an oscillation that reflects the pump-induced generation of pulsed THz radiation (Fig. S3). The spectra of the emitted THz pulses after excitation of 800 nm and 400 nm are identical (Fig. S3). Following the oscillation, the decrease in the signal suggests the recombination of photoexcited charge carriers. The recombination dynamics markedly depend on the carrier density. The recombination dynamics markedly depend on the carrier density. In general, the Auger recombination rate is proportional to the cube of the carrier density,  $R_{Auger} = dN(\tau)/d\tau = -k_3N(\tau)^3$ , where  $N(\tau)$  is the free charge carrier density and  $k_3$  is the Auger coefficient associated with the third-order process.

Since the measured THz differential transmission signal (Figs. 3 and S4) is proportional to the photoinduced conductivity, which is directly proportional to N, fitting the above rate equation to the transients results in the extraction of the Auger coefficient  $k_3$ . This model is

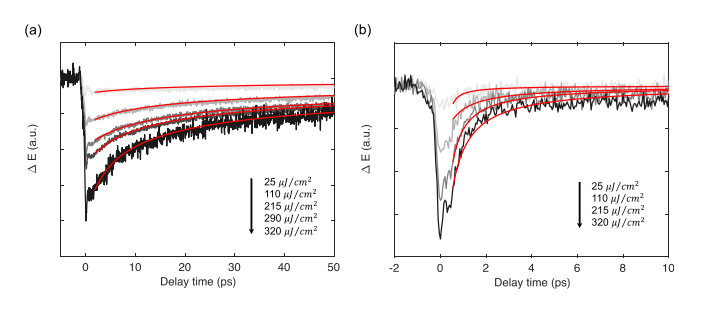


**FIG. 3.** One-dimensional pump scans acquired from  $Re_6Se_8Cl_2$  (a) and  $Mo_6S_3Br_6$  (b) for 800 nm excitation with different pump-fluences. The red curves are the fitted model of a cubic (a) and a quadratic (b) dependence on the charge carrier density. The fluence dependence of the pump-probe dynamics after 400 nm excitation of both materials is presented in Fig. S4.

used to fit the excess carrier relaxation dynamics up to 10 ps, where the effective thickness of the electron gas is limited to the penetration depth, since the contribution from the carrier diffusion is negligible. The effective thickness at a given pump-probe delay  $\tau$  is approximated by the simplest diffusion equation, <sup>28</sup>

$$d(\tau) = \sqrt{\pi D \tau},$$

where D is the diffusion coefficient estimated by the Einstein relation  $D=k_{\rm B}Tm^*/e.^{28,29}$ 

As expected, the third-order process suffices to describe the relaxation dynamics in  $Re_6Se_8Cl_2$  [Fig. 3(a)]. However, in  $Mo_6S_3Br_6$ , the relaxation dynamics deviate significantly from the cubic dependence on the carrier density (Fig. S5), yet displays a quadratic dependence on the carrier density [Fig. 3(b)]. This quadratic dependence is unambiguously concluded by the residuals of the third-order fits (Fig. S5).

The resultant cubic Auger coefficients of bulk  $Re_6Se_8Cl_2$  are presented in Fig. 4(a). At the excitation fluences used here, one could find the monotonic decrease in the Auger coefficient with the excitation density range of  $2\times 10^{18}$  to  $4\times 10^{19}$  cm<sup>-3</sup>. This phenomenon is known to stem from the phase-space filling effect.<sup>30</sup> at low charge densities, the Auger recombination rate has a cubic charge density dependence, owing to the fact that the carrier distribution can be approximated by a Maxwell–Boltzmann distribution. In contrast, at higher densities, where the electron occupation follows the Fermi–Dirac distribution with the limiting value of 1, the cubic dependence of the Auger rate on the carrier density is reduced to quadratic.<sup>30</sup> Thus, the carrier density dependence of the rate coefficient is empirically described by

$$k_3(N) = \frac{k_3^0}{1 + (N/N_0)^b},$$

where  $k_3^0$  is the non-degenerate Auger coefficient at the charge density for  $N \ll N_0$ ;  $N_0$  is the characteristic charge density for the onset of the phase-space filling effect, and b is a dimensionless exponent, usually indicating the degree of degeneracy. In an indirect bandgap semiconductor such as  $\text{Re}_6\text{Se}_8\text{Cl}_2$ , a second-order process via an intermediate state, e.g., the phonon-assisted Auger recombination process, could play an important role in fulfilling the combined energy and momentum conservation restriction. The effective lifetime  $[T=N/(dN/d\tau)]$  for  $\text{Re}_6\text{Se}_8\text{Cl}_2$  after both 800 and 400 nm excitation is obtained to be  $\sim$ 20 ps regardless of the excitation density (Fig. S6). It

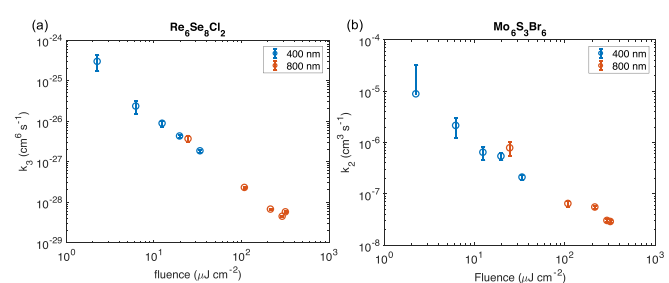


**FIG. 4.** The third-order rate coefficients of  $Re_6Se_8Cl_2$  (a) and the second-order rate coefficients of  $Mo_6S_3Br_6$  (b) extracted from the data shown in Fig. 3 using the recombination rate model, plotted as a function of injected photocarrier density upon 400 nm (blue) and 800 nm (orange) excitations. The error bars represent the 95% confidence intervals of the fitting parameters.

is noteworthy that InN, one of the leading materials for LED and lasers,  $^{33,34}$  has the Auger lifetimes reported to vary from 20 to 2000 ps in the carrier density range, the same as our experimental condition  $(10^{18}-10^{19} {\rm cm}^{-3}).^{35-38}$ 

In Mo<sub>6</sub>S<sub>3</sub>Br<sub>6</sub>, the quadratic dependence of the relaxation dynamics on the carrier density is shown in Fig. 3(b). Again, the rate coefficient also monotonically decreases with the carrier density [Fig. 4(b)]. The second-order relaxation process indicates either a rate-limiting Auger process or radiative band-to-band recombination. The ratelimiting Auger process could be caused by high levels of doping or defects, in such a way that the Auger rate has a linear<sup>39</sup> or quadratic<sup>15</sup> dependence on the carrier density already at low photoinjected carrier densities. With increasing photoinjected carrier density, phase-space filling effects lead to the monotonic decrease in the Auger rate coefficient, similar to the case of  $Re_6Se_8Cl_2$  (Fig. 4).  $^{30}$  The contribution of the band-to-band recombination seems to be negligible, given the subpicosecond lifetime in Mo<sub>6</sub>S<sub>3</sub>Br<sub>6</sub>. The band-to-band recombination occurs with typical lifetimes of hundreds of picoseconds to a few nanoseconds in semiconductors of reduced dimensionality, such as transition metal dichalcogenides (TMDs),<sup>40</sup> 2D quantum wells,<sup>41</sup> and 1D quantum wires. 42 On the other hand, the rate-limiting Auger recombination times facilitated by defects in TMDs are reported to be in the subpicosecond to a few picoseconds range.<sup>43</sup> Since we observe free charge carriers as the major photoproducts, we rule out notable contributions from the exciton-exciton annihilation process. Excitation of Mo<sub>6</sub>S<sub>3</sub>Br<sub>6</sub> by 400 and 800 nm pulses gives a constant effective lifetime of  $\sim$ 0.5 ps (Fig. S6), several orders of magnitude shorter compared to Re<sub>6</sub>Se<sub>8</sub>Cl<sub>2</sub>, which also supports the high level of dopant/defect density.

In summary, we have investigated the ultrafast carrier dynamics of two representative  $Re_6Se_8Cl_2$  and  $Mo_6S_3Br_6$  2D superatomic solid semiconductors at high excitation densities. The chemical differences between the two materials strongly affect the Auger-assisted relaxation dynamics, illustrating the prospects of chemically engineering superatomic solid semiconductors to suppress non-radiative losses.

See the supplementary material for sample preparation; additional Lorentzian fit of photoconductivity spectra in Fig. 2; photoconductivity spectra with the Drude–Smith model of  $Mo_6S_3Br_6$  at room temperature; the observed pump-induced THz generation/emission; pump-probe scans after  $400\,\mathrm{nm}$  excitation; comparison between the cubic dependence and quadratic dependence models for describing pump-probe scans in  $Mo_6S_3Br_6$ ; and the estimated effective lifetimes of photocarriers.

Time-resolved spectroscopy measurements and analyses at Max Planck Institute for Polymer Research were financially supported by the Max Planck Society. Materials synthesis and characterization at Columbia University were supported by the Center for Precision Assembly of Superstratic and Superatomic Solids, a Materials Science and Engineering Research Center (MRSEC) through NSF Grant No. DMR-1420634 and by the NSF CAREER award through Grant No. DMR-1751949 (X.R.). A.D. is supported by the NSF GRFP (DGE 16-44869). This work was also supported in part by the U.S. Air Force Office of Scientific Research (AFOSR Award No. FA9550-18-1-0020). The authors thank Rüdiger Berger, Kaloyan Koynov, and Wentao Zhang for insightful discussions and supplementary measurements.

The authors declare no competing financial interest.

### **REFERENCES**

- <sup>1</sup>X. Roy, C. Lee, A. C. Crowther, C. L. Schenck, T. Besara, R. A. Lalancette, T. Siegrist, P. W. Stephens, L. E. Brus, P. Kim, M. L. Steigerwald, and C. Nuckolls, Science 341, 157 (2013).
- <sup>2</sup>A. Pinkard, A. M. Champsaur, and X. Roy, Acc. Chem. Res. 51, 919 (2018).
- <sup>3</sup>R. Chevrel, P. Gougeon, M. Potel, and M. Sergent, J. Solid State Chem. **57**, 25 (1985).
- <sup>4</sup>M. B. Maple, Ø. Fischer, and H. F. Braun, Superconductivity in Ternary Compounds II: Superconductivity and Megnetism (Springer-Verlag, Berlin, 1982).
- <sup>5</sup>J. Chen, A. J. Millis, and D. R. Reichman, Phys. Rev. Mater. 2, 114801 (2018).
- <sup>6</sup>E. J. Telford, J. C. Russell, J. R. Swann, B. Fowler, X. Wang, K. Lee, A. Zangiabadi, K. Watanabe, T. Taniguchi, C. Nuckolls, P. Batail, X. Zhu, J. A. Malen, C. R. Dean, and X. Roy, e-print arXiv:1906.10785 (2019).
- <sup>7</sup>X. Zhong, K. Lee, B. Choi, D. Meggiolaro, F. Liu, C. Nuckolls, A. Pasupathy, F. De Angelis, P. Batail, X. Roy, and X. Zhu, Nano Lett. 18, 1483 (2018).
- <sup>8</sup>X. Zhong, K. Lee, D. Meggiolaro, A. H. Dismukes, B. Choi, F. Wang, C. Nuckolls, D. W. Paley, P. Batail, F. De Angelis, X. Roy, and X. Y. Zhu, Adv. Funct. Mater. 29, 1902951–1902951 (2019).
- <sup>9</sup>D. Certain and R. Lissillour, Z. Phys. D 3, 411 (1986).
- <sup>10</sup>V. E. Fedorov, A. V. Mishchenko, and V. P. Fedin, Russian Chemical Reviews 54, 408 (1985).
- <sup>11</sup>B. Choi, K. Lee, A. Voevodin, J. Wang, M. L. Steigerwald, P. Batail, X. Zhu, and X. Roy, J. Am. Chem. Soc. 140, 9369 (2018).
- <sup>12</sup>Q. H. Wang, K. Kalantar-Zadeh, A. Kis, J. N. Coleman, and M. S. Strano, Nat. Nanotechnol. 7, 699 (2012).
- <sup>13</sup>J. S. Ross, P. Klement, A. M. Jones, N. J. Ghimire, J. Yan, D. G. Mandrus, T. Taniguchi, K. Watanabe, K. Kitamura, W. Yao, D. H. Cobden, and X. Xu, Nat. Nanotechnol. 9, 268 (2014).
- <sup>14</sup>B. W. H. Baugher, H. O. H. Churchill, Y. Yang, and P. Jarillo-Herrero, Nat. Nanotechnol. 9, 262 (2014).
- 15T. Chlouba, F. Trojánek, J. Laube, D. Hiller, S. Gutsch, M. Zacharias, and P. Malý, Sci. Rep. 8, 1703 (2018).
- <sup>16</sup>J. Piprek, Phys. Status Solidi A **207**, 2217 (2010).
- <sup>17</sup>G. Verzellesi, D. Saguatti, M. Meneghini, F. Bertazzi, M. Goano, G. Meneghesso, and E. Zanoni, J. Appl. Phys. 114, 71101 (2013).
- 18 P. U. Jepsen, D. G. Cooke, and M. Koch, Laser Photonics Rev. 5, 124 (2011).
- <sup>19</sup>R. E. Glover III and M. Tinkham, *Phys. Rev.* **108**, 243 (1957).
- <sup>20</sup>N. Mott, J. Solid State Chem. **88**, 5 (1990).
- <sup>21</sup>M. Combescot, Phys. Status Solidi B **86**, 349 (1978).
- <sup>22</sup>R. Ulbricht, E. Hendry, J. Shan, T. F. Heinz, and M. Bonn, Rev. Mod. Phys. 83, 543 (2011).
- <sup>23</sup>N. V. Smith, Phys. Rev. B **64**, 155106 (2001).
- <sup>24</sup>E. Hendry, M. Koeberg, J. Pijpers, and M. Bonn, Phys. Rev. B 75, 233202 (2007).
- 25 T. T. Mnatsakanov, M. E. Levinshtein, A. G. Tandoev, S. N. Yurkov, and J. W. Palmour, J. Appl. Phys. 97, 103715 (2005).
- <sup>26</sup>T. T. Mnatsakanov, V. B. Shuman, L. I. Pomortseva, D. Schröder, and A. Schlögl, Solid. State. Electron. 44, 383 (2000).
- <sup>27</sup>P. Cunningham and L. Hayden, J. Phys. Chem. C **112**, 7928 (2008).
- <sup>28</sup>Z. Mics, A. D'Angio, S. A. Jensen, M. Bonn, and D. Turchinovich, Appl. Phys. Lett. **102**, 231120 (2013).
- <sup>29</sup>S. M. Sze, Semiconductor Devices, Physics and Technology (Wiley, New York, 1985).
- 30 J. Hader, J. V. Moloney, and S. W. Koch, Appl. Phys. Lett. 87, 201112 (2005).
- 31 E. Kioupakis, Q. Yan, D. Steiauf, and C. G. Van De Walle, New J. Phys. 15, 125006 (2013).
- 32 A. Haug, J. Phys. Chem. Solids 49, 599 (1988).
- 33 A. McAllister, D. Bayerl, and E. Kioupakis, Appl. Phys. Lett. 112, 251108 (2018).
- <sup>34</sup>C. J. Humphreys, MRS Bull. 33, 459 (2008).
- 35T.-R. Tsai, C.-F. Chang, and S. Gwo, Appl. Phys. Lett. 90, 252111 (2007).
- <sup>36</sup>D.-J. Jang, G.-T. Lin, C.-L. Hsiao, L. W. Tu, and M.-E. Lee, Appl. Phys. Lett. 92, 042101 (2008).
- <sup>37</sup>Y. Cho, X. Lue, M. Wienold, M. Ramsteiner, H. T. Grahn, and O. Brandt, Phys. Rev. B 87, 155203 (2013).

 <sup>&</sup>lt;sup>38</sup>F. Chen, A. N. Cartwright, H. Lu, and W. J. Schaff, Phys. Status Solidi 202, 768 (2005).
 <sup>39</sup>K. W. Williams, N. R. Monahan, T. J. S. Evans, and X. Y. Zhu, Phys. Rev. Lett. 118, 087402 (2017).

Ho, 00/402 (2017).
 H. Wang, C. Zhang, W. Chan, C. Manolatou, S. Tiwari, and F. Rana, Phys. Rev. B 93, 45407 (2016).

A. Hangleiter, Phys. Rev. B 48, 9146 (1993).
 Bellessa, V. Voliotis, R. Grousson, X. L. Wang, M. Ogura, and H. Matsuhata,

Phys. Rev. B **58**, 9933 (1998).

43H. Wang, J. H. Strait, C. Zhang, W. Chan, C. Manolatou, S. Tiwari, and F. Rana, Phys. Rev. B **91**, 165411 (2015).